Bioactive Materials 35 (2024) 401–415

Contents lists available at ScienceDirect

Bioactive Materials

journal homepage: www.keaipublishing.com/en/journals/bioactive-materials

Development of ovalbumin implants with different spatial configurations for treatment of peripheral nerve injury

Tiantian Zheng [a,b], Hongxia Gao [a], Yaqiong Liu [a], Shaolan Sun [a], Wenchao Guan [a], Linliang Wu [c], Yumin Yang [a,*], Guicai Li [a,**]

[a] Key Laboratory of Neuroregeneration, Co-innovation Center of Neuroregeneration, Nantong University, Nantong, 226001, China
[b] National Engineering Research Center for Biomaterials, Sichuan University, Chengdu, 610065, China
[c] The People's Hospital of Rugao, Affiliated Hospital of Nantong University, 226599, Nantong, China

ARTICLE INFO

Keywords:
Ovalbumin
Casting method
Electrospinning
Freeze drying
Nerve scaffold
Peripheral nerve injury

ABSTRACT

Peripheral nerve injury (PNI) seriously affects the health and life of patients, and is an urgent clinical problem that needs to be resolved. Nerve implants prepared from various biomaterials have played a positive role in PNI, but the effect should be further improved and thus new biomaterials is urgently needed. Ovalbumin (OVA) contains a variety of bioactive components, low immunogenicity, tolerance, antimicrobial activity, non-toxicity and biodegradability, and has the ability to promote wound healing, cell growth and antimicrobial properties. However, there are few studies on the application of OVA in neural tissue engineering. In this study, OVA implants with different spatial structures (membrane, fiber, and lyophilized scaffolds) were constructed by casting, electrospinning, and freeze-drying methods, respectively. The results showed that the OVA implants had excellent physicochemical properties and were biocompatible without significant toxicity, and can promote vascularization, show good histocompatibility, without excessive inflammatory response and immunogenicity. The in vitro results showed that OVA implants could promote the proliferation and migration of Schwann cells, while the in vivo results confirmed that OVA implants (the E5/70% and 20 kV 20 μL/min groups) could effectively regulate the growth of blood vessels, reduce the inflammatory response and promote the repair of subcutaneous nerve injury. Further on, the high-throughput sequencing results showed that the OVA implants up-regulated differential expression of genes related to biological processes such as tumor necrosis factor-α (TNF-α), phosphatidylinositide 3-kinases/protein kinase B (PI3K-Akt) signaling pathway, axon guidance, cellular adhesion junctions, and nerve regeneration in Schwann cells. The present study is expected to provide new design concepts and theoretical accumulation for the development of a new generation of nerve regeneration implantable biomaterials.

1. Introduction

PNI caused by wars, traffic accidents, natural disasters, surgeries, etc. Lead to impaired mobility, sensory deficits and loss of function, thus seriously affecting the physical and mental health of the patients and imposing a serious economic burden on their families and society [1]. Therefore, repair and functional reconstruction after PNI is one of the major problems to be solved in clinical practice [2] However, autologous nerve grafts, which are the "gold standard" for peripheral nerve injury repair, are limited in clinical application due to their limited source and size mismatch [3] Currently, various tissue-engineered nerve implants have been utilized to achieve the repair of nerve injury [4,5], and a large number of studies have focused on the selection of biomaterials [6,7]. Among them, the natural biopolymers or synthetic polymers are the commonly used materials for nerve implants [8], which have been used to fabricate different types of nerve implants, including membrane, electrospinning fiber, hydrogel and sponge scaffolds, etc [9,10]. Although synthetic polymer materials can provide better mechanical properties for grafts, natural biomaterials are less toxic, more bioactive and biocompatible, and can better activate cell

Peer review under responsibility of KeAi Communications Co., Ltd.
* Corresponding author.
** Corresponding author.
E-mail addresses: yangym@ntu.edu.cn (Y. Yang), gcli1981@ntu.edu.cn (G. Li).

https://doi.org/10.1016/j.bioactmat.2024.01.025
Received 29 December 2023; Received in revised form 25 January 2024; Accepted 27 January 2024

proliferation and migration [11] However, although artificial nerve implants have achieved remarkable results in nerve tissue engineering, they are still not as effective as autologous grafts and do not fully meet the clinical needs. Therefore, there is an urgent need to develop new nerve implants materials for better treatment and repair of PNI.

Among the various polymers that can be used to prepare artificial implants, natural polymers with high bioactivity and biocompatibility, easy handling and low production costs are preferred [12]. Currently, the protein-based natural polymers have been widely used in tissue engineering due to their similarity to natural extracellular matrix components [13]. Although protein-based biomaterials support cell attachment, proliferation, migration, etc. More than other materials, their limited sources and complex extraction and purification procedures make them expensive or difficult to obtain [14]. Egg white, as a combination of proteins and growth factors, is a low-cost, readily available, direct protein-based biomaterial, and can mediate cell adhesion and growth [15]. Moreover, it also has excellent biological functions such as antibacterial and anti-inflammatory, promotes cell adhesion, stimulates nerve cell growth, and is rich in trophic factor [16]. Among them, OVA, a glycoprotein extracted from egg white, is the most abundant protein (54%) in egg white, and has genetic similarity to human serum albumin [17]. OVA has been used for centuries as an excipient in creams for the treatment of various diseases due to its non-immunogenicity, tolerance, antimicrobial activity, non-toxicity and biodegradability [17,18]. In addition, OVA has excellent biocompatibility, promotes cell attachment and proliferation, and can be degraded in vivo into safe by-products, thus OVA has been used in the repair of bone and soft tissue injuries [19,20]. OVA contains a variety of bioactive components, so it has wound healing promotion, cell growth and antimicrobial properties. It is worth mentioning that egg white can mimic the effect of nerve growth factor (NGF) by inducing axon growth in mammalian cells such as PC12 cells, which suggests that bioactive components are similar to NGF may also present in OVA [16,21]. Therefore, the development of OVA nerve implants is expected to provide continuous nutrient delivery for long-term growth of nerve tissues, but at present, studies on the application of OVA in the repair of PNI have not been reported.

It has been found that the spatial structure of the scaffolds possesses a significant impact on the neuroregeneration outcome [9]. Currently, the construction of tissue-engineered neural implants with different spatial structure, such as porous scaffolds, hydrogel, membrane, fiber and nanogels can be achieved using various processing and fabrication methods, e.g. freeze-drying, electrostatic spinning, solution casting, and phase separation, etc [22–24]. The advantage of freeze-drying is that the pore size and porosity can be controlled by changing the parameters of freezing, and the implants obtained have high porosity and interconnected structure, which is conducive to the retention of the physical and chemical properties of the implant material [25,26]. We previously prepared porous chitosan conduit with longitudinally aligned structures on the intraluminal wall using the freeze-drying method, and the conduit was proved to significantly promote the regeneration of sciatic nerves in the 10 mm gap of the rat [27]. Preparation of micro/nano fiber scaffolds by electrospinning has been widely used in tissue engineering [28,29]. Nanofiber structures are more conducive to cell adhesion and proliferation as well as loading of bioactive factors than micron-sized fiber structures [30,31]. In addition, nanoscale fibers prepared by electrospinning can mimic the extracellular matrix microenvironment of tissues and thus better modulate cell behaviors [8,32,33]. Li et al. successfully prepared a biomimetic microenvironment-inspired scaffold integrating anisotropic micro-nanocomposite topology grafted with IKVAV peptide through micro-molding, electrostatic spinning technology and surface biomodification, the scaffolds were proven to effectively promote peripheral nerve regeneration [34]. Solution casting is the simplest and most economical method of preparing nerve implants. Generally, a solvent is used to dissolve the polymer material, with the addition of a porogenic agent or granules as required, and the mixture is injected into a mold of the desired geometry, then the solvent is evaporated to form a membrane [35,36]. Based on the above mentioned, nerve implants with different spatial structures can be prepared using different processing and fabrication techniques, but there are few reports on what kind of spatial structure of OVA implants can more effectively promote the repair of PNI.

In this study, OVA implants with different spatial structures (solid membrane, porous sponge scaffolds, and fibrous scaffolds) were prepared and compared for the treatment of PNI (Fig. 1). Firstly, OVA membrane, OVA fiber scaffolds, and OVA sponge scaffolds were prepared using casting, electrospinning, and freeze-drying methods. Then, the physical properties, surface morphology and compositional structure of the OVA implants were analyzed, respectively. Next, the biocompatibility was evaluated. Then, through the above experiments, two groups of each form of implants were optimally selected for comparison of the pro-vascularization, inflammatory response, histocompatibility and immunogenicity. Further on, the effect of nerve regeneration during tissue healing after PNI was evaluated. Finally, high-throughput sequencing and molecular biology experiments were used to preliminarily reveal the mechanism of OVA implants on the regulation of nerve regeneration. It is expected that such artificial OVA nerve implants may be potential candidates for clinical use in peripheral nerve regeneration. The study will provide a more ideal biomaterial scaffolds for the repair of PNI in future.

2. Results

2.1. 1-(3-Dimethylaminopropyl)-3-ethylcarbodiimide hydrochloride (EDC) cross-linked OVA scaffolds

The changes in the characteristic peaks of OVA scaffolds before and after cross-linking were detected by fourier transform infrared (FTIR) spectroscopy, and the results are shown in Fig. 2A. The peaks at 1525 cm^{-1} and 1539 cm^{-1} indicated the formation of C═N double bonds in all samples and their intensity decreased as the samples were cross-linked. The characteristic *N*–H peak of OVA was detected at wavelength 3394 cm^{-1}, the peak present at 3400 cm^{-1} was a type II amine bond, and the peak at wavelength 1468 cm^{-1} indicated the formation of *C*–N bonds in all samples, and its intensity increased with the cross-linking of the samples. The results showed that all groups of OVA scaffolds were successfully crosslinked by EDC. The results of Fig. 2B and C indicated the presence of characteristic peaks of OVA at approximately 3282, 1640, and 1520 cm^{-1} representing amide A (*N*–H stretching), amide I (C═O stretching), and amide II (*N*–H bending), respectively. No additional characteristic peaks were observed when the OVA sample was dissolved using acetic acid. A slight increase in the amide I and amide II bands was observed in the spectra due to the hydrocarbon stretching vibrations of the CH_2 and CH_3 groups. In addition, X-ray photoelectron spectroscopy (XPS)tests were performed on the OVA scaffolds before and after cross-linking with 5 mM EDC and 70% ethanol to analyze the change in binding energy. As shown in the results of Fig. 2D, the content of carbon increased while the content of oxygen decreased after cross-linking. The binding energies of C and S elements before and after cross-linking of OVA scaffolds were analyzed, and the results showed that the C═O, *C*–O and *C*–C/C═C bonds were still retained, the content of sulfur did not change significantly before and after cross-linking.

2.2. Characterization of OVA implants with different spatial structures

The parameters of OVA membrane, fiber, and sponge scaffolds prepared by casting, electrospinning, and freeze-drying methods are shown in Tables S1–3, respectively. For OVA membranes, as shown in Fig. S1A, OVA membranes prepared after cross-linking with 50% and 70% ethanol yielded intact membranes and the completion of the cross-linking altered the water-soluble properties of the OVA membranes. The OVA membranes obtained after cross-linking with 100% ethanol were poorly flexible and not easy to obtain the complete membrane. The

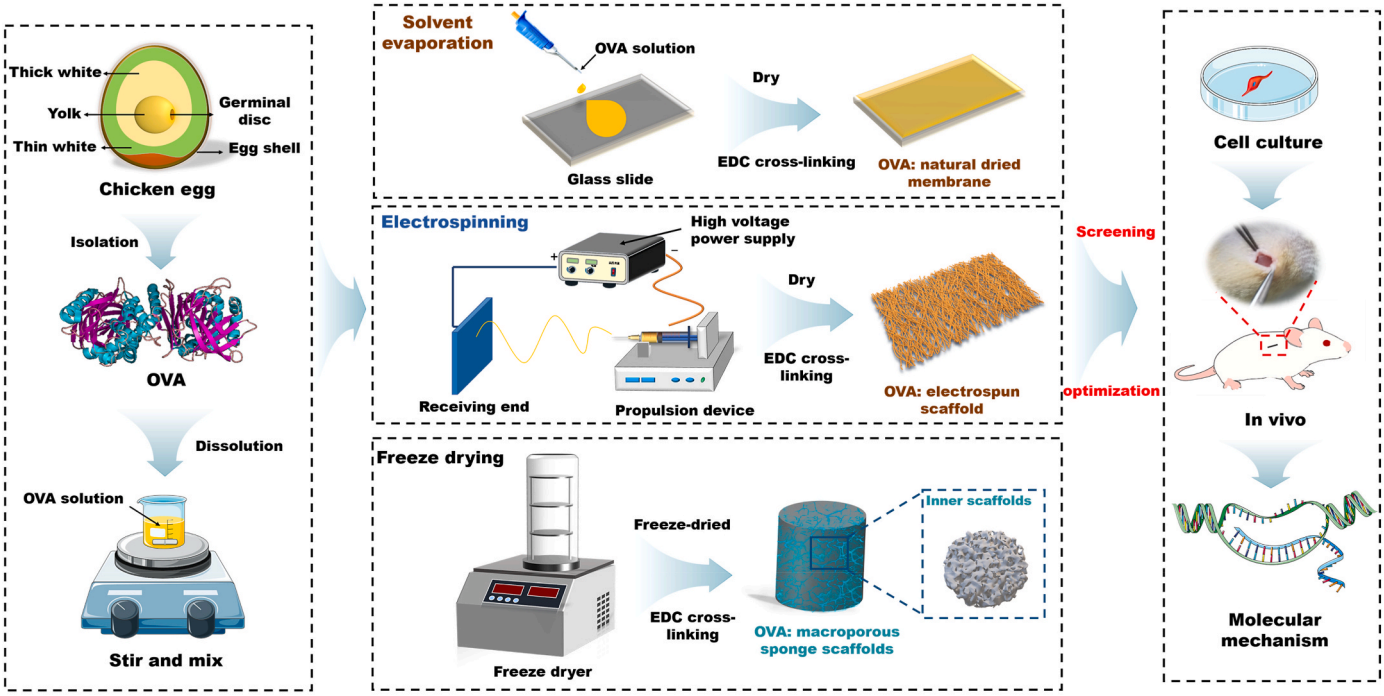

Fig. 1. Sketch map of the preparation of OVA implants with different spatial structures (membrane, fiber, and lyophilized scaffold).

results of UV spectroscopy are shown in Fig. S1B. The transparency of the membrane after crosslinking with 70% ethanol was significantly higher than that of the 50% ethanol group. The transparency of the OVA membrane was changed by varying the concentration of EDC at the same ethanol concentration. After crosslinking with 5 mM EDC, the transparency of the membrane was higher than that of 1 mM and 10 mM EDC concentrations. The UV spectral scanning results showed that the highest transparency of the OVA membrane was obtained after crosslinking with 5 mM EDC and 70% ethanol. The membrane with high transparency will be favorable for observing the wound healing. Fig. 3A shows that the surface of the uncrosslinked OVA membrane was uneven and had more folds. The surface of the E5/70% and E10/70% OVA membranes was relatively flat and contained a small number of air holes. As shown in Fig. 3D, the overall trend of the swelling rate of the six groups of OVA membranes gradually increased within 12 h and finally reached equilibrium with the extension of time. After 12 h, the swelling rate of E1/70% was the highest compared with the other groups, and E10/50% group showed lower swelling rate, but there was no significant difference among the three groups. Fig. 3E displays that the contact angles of the OVA membrane in each group were less than 75°, indicating the hydrophilicity. The OVA membrane is able to undergo significant elastic strain under the action of external force. Fig. 3F and Fig. S3 show that the elastic modulus and maximum load of the OVA membrane increased with the concentration of cross-linking agent, indicating the mechanical strength of the OVA membrane by the cross-linking agent with concentration dependence.

For OVA fiber scaffolds, when hexafluoroisopropanol (HFIP) and trifluoroacetic acid (TFA) were mixed in the ratio of 2:1, the optimal electrospinning conditions were OVA solution concentration of 10%, electrospinning time of 5 min, receiving distance of 15 cm, and needle gauge of 20#. Varying the voltage (18–25 kV) and the flow rate (12–25 μL/min) under these electrospinning parameter conditions resulted in electrospun fibers with high filament yield, uniform fibers, and no droplet appearance, as shown in Fig. S2A. The better four groups of fibers were further selected for crosslinking and characterization including 20 kV 15 μL/min, 20 kV 20 μL/min, 20 kV 25 μL/min and 25 kV 20 μL/min. As shown in Fig. S2B, the four groups of fiber scaffolds were crosslinked by EDC to improve the stability without changing the surface morphology of the fibers. The nanofibers showed a uniform continuous random distribution, and the statistical analysis of the fiber diameters in Fig. 3B and C showed that the fiber diameters of the 20 kV 15 μL/min and 20 kV 20 μL/min groups averaged 657 nm and 635 nm, whereas the fiber diameters of the 20 kV 25 μL/min group averaged 769 nm comparing with the 25 kV 20 μL/min group, the other three groups of electrospun fibers showed more slender diameters. Fig. 3G shows that the contact angle of all OVA fiber scaffolds was less than 90°, indicating that the OVA fiber scaffolds were hydrophilic and displays a decreasing trend with increasing flow rate under the same voltage conditions.

For OVA sponge scaffolds, the scaffolds had a uniform circular or elliptical aperture, which were uniformly connected to each other throughout the scaffolds. This microstructure is suitable for supporting cell growth and migration. In addition, the pore may also promote angiogenesis and reduce fibrotic response in vivo. As shown in Fig. 3H, I and Fig. S4, the pore size of 6% OVA sponge scaffolds ranged from 20 to 60 μm with an average porosity of 54.48%, while 8% OVA sponge scaffolds had a pore size range of 10–30 μm with an average porosity of 45.44%, which significant decreased compared to 6% OVA sponge scaffolds. Therefore, 8% OVA sponge scaffolds were selected for subsequent experiments. In Fig. 3J, N and Fig. S5, the stress-strain curves showed that the OVA sponge scaffolds crosslinked with different concentrations of EDC had good mechanical properties, and was able to undergo significant elastic strain under the action of external forces. The elastic modulus of the OVA sponge scaffolds increased with EDC concentration. Moreover, the OVA sponge scaffolds of E4 and E2 groups remained structurally intact even after subjected to 50 compression tests. However, in the E0.5 group, the structure of the scaffolds was damaged after the 20th compression. The initial height of the three groups of OVA sponge scaffolds was 0.5 cm before testing, and was about 0.2 cm after the initial compression test, then the scaffolds recovered to their original state quickly after being put into PBS, which indicated that the OVA scaffolds showed good shape memory properties. E4 group was able to recover to its original state after 50 compression tests, while E2 group recovered to its original state only in the initial 10 cycle tests, and its structure was damaged and irreversible in the

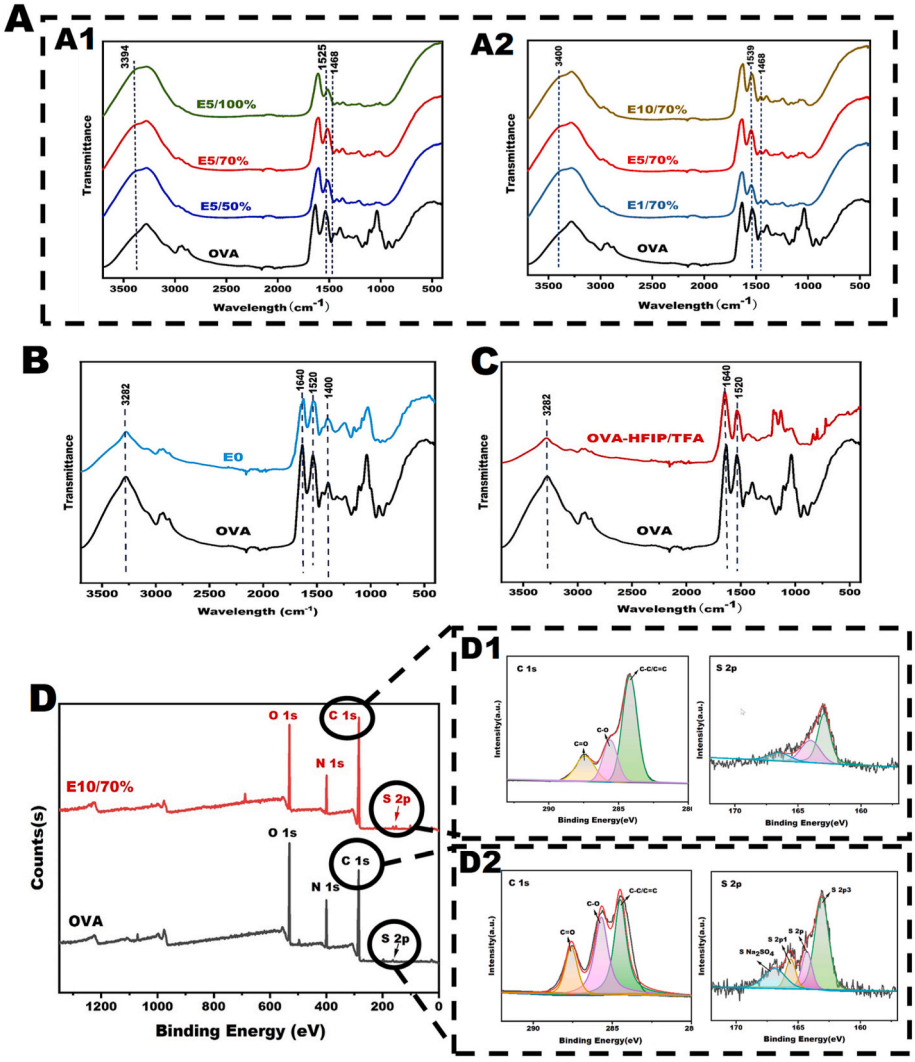

Fig. 2. Chemical characterization of EDC cross-linked OVA scaffold. (A) FTIR Spectra of OVA Membrane Crosslinked with EDC and ethanol, A1: OVA membrane cross-linked with 5 mM EDC and different concentrations of ethanol, A2: OVA membrane crosslinked with different concentrations of EDC and 70 % ethanol, (B) FTIR spectra of OVA fiber scaffold, (C) FTIR spectra of OVA Sponge Scaffold, (D) Full spectra of XPS test, D1: High-resolution spectra of C1s and S1s elements in E10/70% group, D2: OVA group.

subsequent tests. The compression test results show that the concentration of cross-linking agent affected the compressive strength of OVA scaffolds. The results in Fig. 3K show that among the six groups of sponge scaffolds, E2 group had the smallest contact angle and the best hydrophilicity. The results in Fig. 3L and M show that the degradation rate of the sponge scaffolds could be adjusted by adjusting EDC cross-linking agent. Within 21 days, all five groups of sponge scaffolds showed degradation behavior, with the highest degradation rate in group E1. And with the increase of crosslinker concentration, the degradation rate of sponge scaffolds gradually increased, reaching the maximum value at group E1 (≈3.4 times of the initial weight).

2.3. *In vitro* bioevaluation

The cytotoxicity of the OVA implants was evaluated by 3- (4,5)-dimethylthiahiazo(-z-y1)-3,5-di-phenytetrazoliumromide (MTT) assay after culturing the L929 cell line for 24 h using the extracts of OVA membranes for 1 d and 3 d, as shown in Fig. 4A. The results showed that the cell viability of all OVA implants was greater than 90% compared with the control group, indicating no significant cytotoxicity and suitable for subsequent cell cultures. The cell viability of each group at 3 d was overall higher than that of 1 d. Schwann cells were then cultured on the OVA membrane, and cell viability assays were performed after 1 and 3 d of culture. As shown in Figs. S6–7, the number of live cells on the OVA membranes of each group was significantly higher than the dead cells, and the cells were evenly distributed on the membrane surface, almost no dead cells were observed in the experimental group. The results of live-dead staining further indicated that the OVA membrane was not cytotoxic. The hemolytic performance of the OVA membranes was evaluated by in vitro hemolysis rate assay. The results in Fig. 4B and C showed that there was no difference in color between the experimental groups and the control group, and the hemolysis rate of all OVA membranes was less than 1%, indicating all OVA membrane were not easy to cause hemolysis.

As shown in Fig. 4D–F, Schwann cells grew poorly in the E10/50% group with low cell number, but grew better in other OVA membranes, and the cells were easy to aggregate in the E1/50% and E5/50% groups. However, in the E1/70%, E5/70% and E10/70% groups, the cell distribution was uniform and the cell morphology was good, and the cell distribution in the E5/70% and E10/70% groups was more and the growth morphology was better than that in the other groups, which further proved that the OVA membrane was biocompatible and suitable for cell growth and proliferation. After culturing Schwann cells on the OVA fiber scaffolds for 3 d, toluidine blue O (TBO) staining was

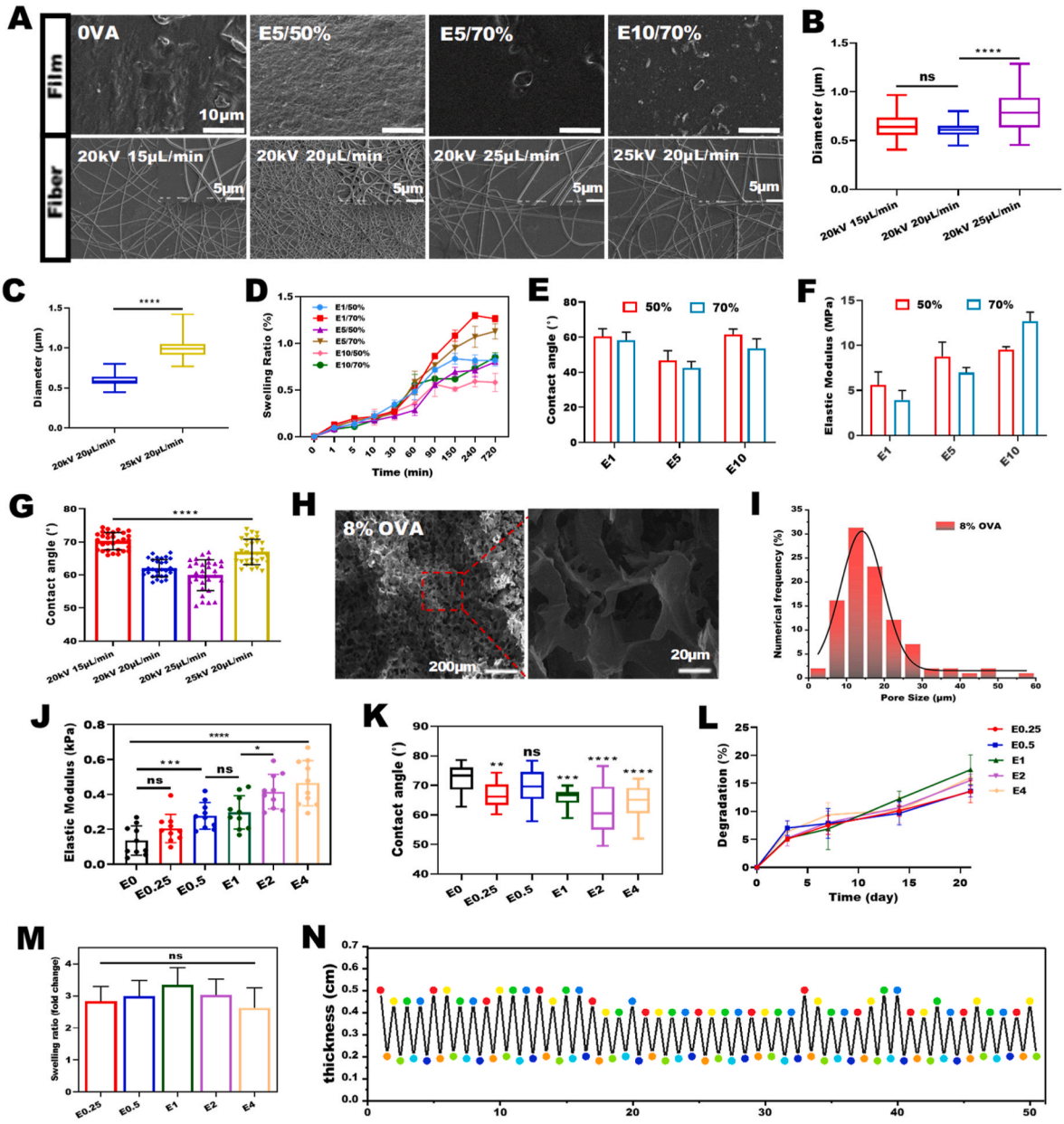

Fig. 3. Physical characterization of OVA implants with three forms. (A) SEM observation of OVA membrane and fiber, (B) Statistical results of OVA fiber diameter at different flow rates, n = 30 (C) Statistical results of OVA fiber diameter at different voltages, n = 30 (D) Swelling ratio test of OVA membrane, n = 3 (E) Quantitative analysis of contact angle of OVA membrane, n = 30 (F) Statistics of elastic modulus of OVA membrane before and after crosslinking, n = 5 (G) Quantitative statistical analysis of contact angle of OVA fiber scaffolds, n = 30 (H) SEM observation of 8% OVA sponge scaffolds, (I) Quantitative analysis of pore size of sponge scaffolds, (J) Elastic modulus statistics of sponge scaffolds, n = 5 (K) Quantitative statistical analysis of contact angle of OVA sponge scaffolds, n = 28 (L) Degradation rate of OVA sponge scaffolds, n = 5 (M) Swelling rate of sponge scaffolds, n = 3 (N) 50-cycle compression test of E4 sponge scaffold. Data are shown as means ± SD. Statistical analysis: ***$p < 0.001$, ****$p < 0.0001$, *ns* no significance.

performed, shown in Fig. 4G–I, Schwann cells were evenly distributed on the OVA fiber scaffolds and had good cell morphology. Scanning electron microscopy (SEM) results in Fig. S8 showed that the 20 kV 20 μL/min and 20 kV 25 μL/min had better cell growth morphology and more cells than the other groups. The cell morphology, distribution and infiltration of Schwann cells were additionally evaluated 7 days after incubation on E2 sponge scaffolds. Fig. 4J shows the stained image of the middle cross-section part of the sponge scaffold, which showed that Schwann cells migrated inside the pores of the sponge scaffold and the cell growth status inside the pores was good, indicating that the three-dimensional mesh structure of the sponge scaffolds were favorable for the culture of Schwann cells.

2.4. Subcutaneous inflammation reaction

To evaluate the safety and biocompatibility of OVA implants (membrane, fiber scaffolds, and sponge scaffolds) in vivo, the subcutaneous implantation surgeries in ICR mice performed for one week and two weeks, and the degree of local inflammatory reactions in the tissues was detected by hematoxylin and eosin (H&E) staining, immunofluorescence staining, and enzyme-linked immunosorbent assay (ELISA). As shown in Fig. S9, the green triangles represented the OVA implants and the blue circles were the surrounding tissues. More cellular infiltration into the inner interstitial space of the scaffolds could be observed in the H&E staining images in the 20 kV 20 μL/min, 20 kV 25 μL/min, E2, and E4 groups, whereas more cellular nuclei were observed to be distributed

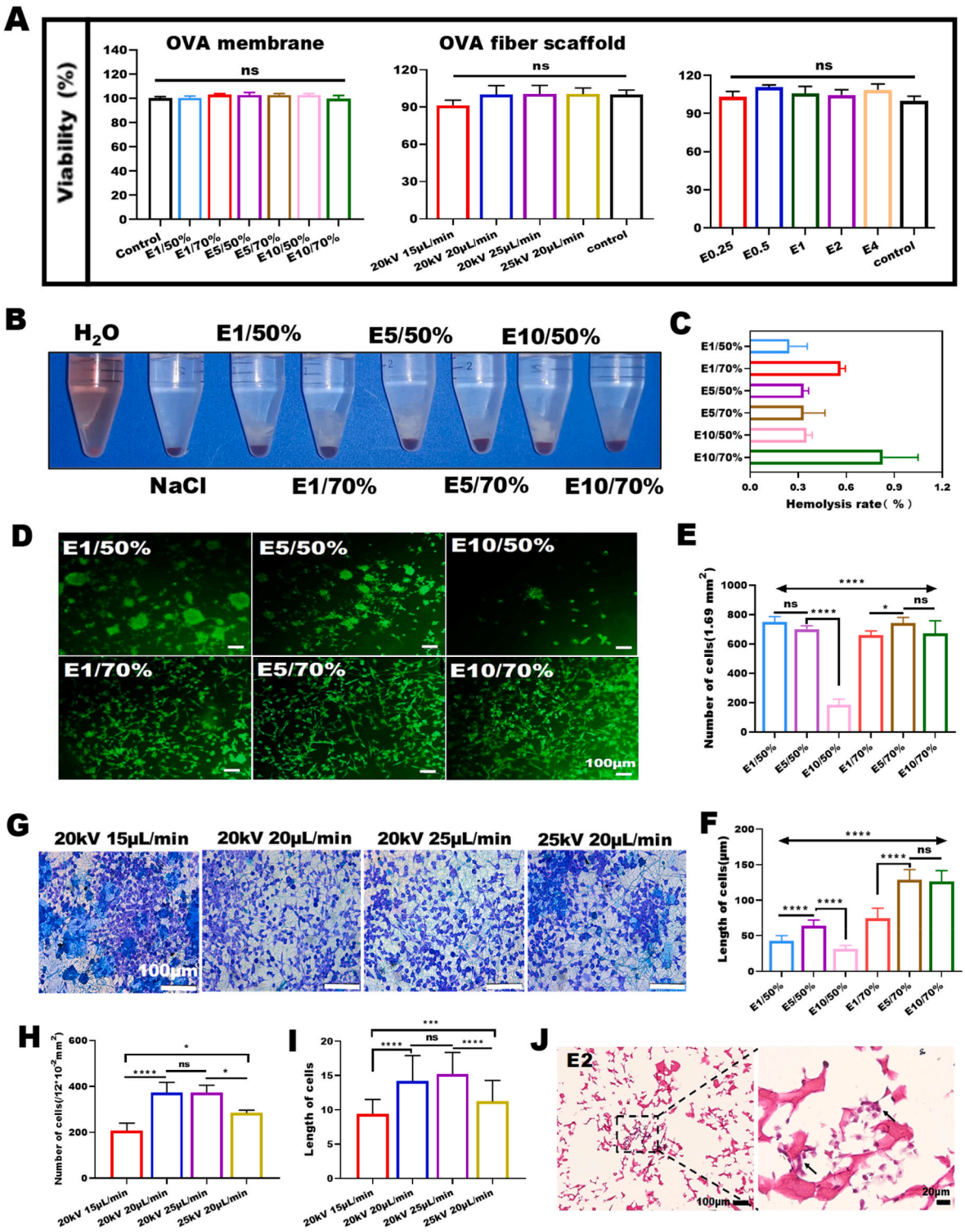

Fig. 4. Biocompatibility evaluation of OVA implants with three forms. (A) Cell viability statistics of OVA scaffolds with three forms, n = 6 (B) Photo of different OVA membranes incubated with red blood cells, (C) Hemolysis rate statistics, n = 6 (D) Immunofluorescence images of RSC96 cells grown on different OVA membranes for 3 days, (E) Number of Schwann cells, n = 5 (F) Statistics of cell differentiation length, n = 30 (G) TBO staining images of RSC96 cells on OVA fiber scaffolds, (H) Number of Schwann cells, n = 5 (I) Differentiation length of Schwann cells, n = 30 (J) H&E staining images of E2 group sponge scaffolds cross section. Data are shown as means ± SD. Statistical analysis: $*p<0.05$, $***p<0.001$, $****p<0.0001$, *ns* no significance.

on the outer edges of the grafts, in E5/70% and E10/70%, respectively, rather than in the grafts. The fluorescence intensity of CD86 in Figs. S10A–C was significantly lower than that of the normal group in both the E10/70% and 20 kV 20 μL/min groups, and the fluorescence intensity of CD86 was slightly lower than that of the normal group in both the E5/70% and 20 kV 25 μL/min groups, but there was no significant difference from the normal group. In contrast, the one-week CD163 fluorescence intensity of the experiment group was significantly higher than that of the normal group. As shown in Fig. 5A–C, the two-week CD86 staining fluorescence intensity of the 20 kV 25 μL/min

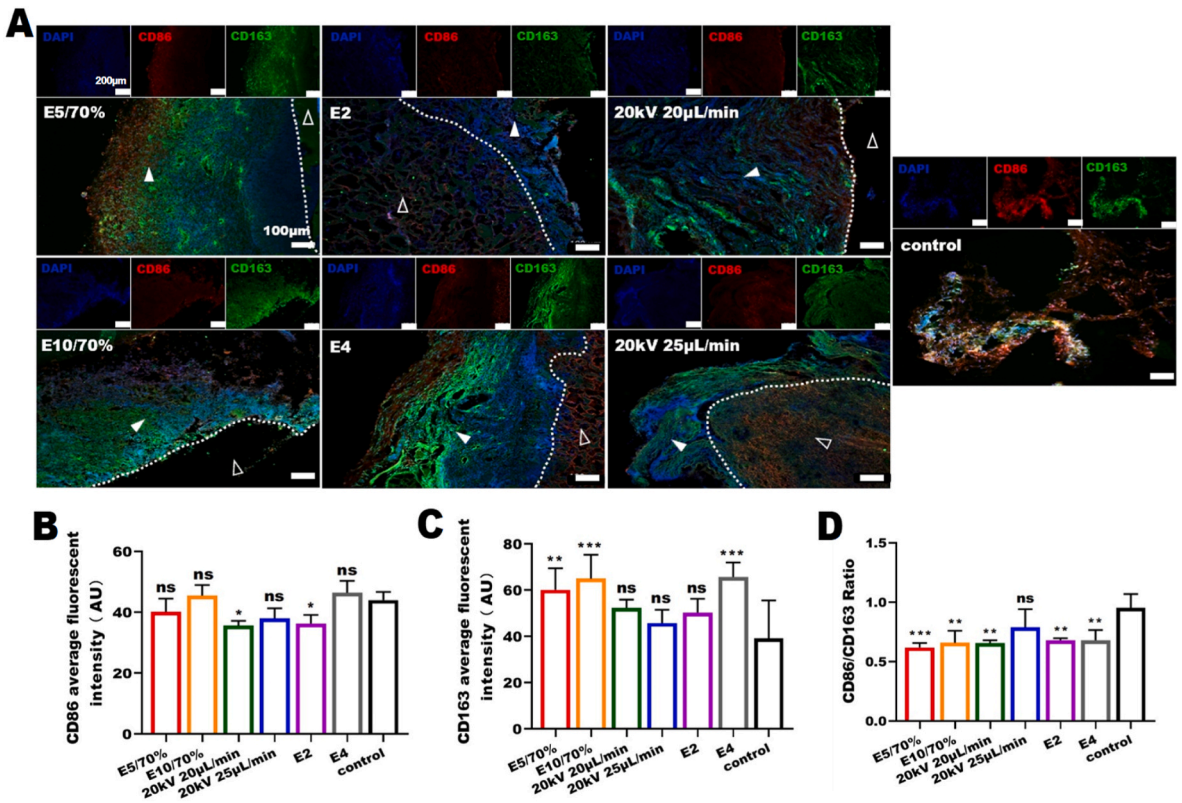

Fig. 5. Subcutaneous inflammation reaction of the OVA implants for 2 weeks, including E5/70%, E10/70%, 20 kV 20 μL/min, 20 kV 25 μL/min, E2, E4 and normal tissue, respectively. (A) Macrophage immunofluorescence images of subcutaneous implants for two weeks, the dashed line represents the dividing line between the scaffold and the surrounding tissue. The solid triangle and the hollow triangle represent the surrounding tissue and the implanted scaffold, respectively. (B) CD86 average immunofluorescence intensity statistics, n = 5 (C) CD163 average immunofluorescence intensity statistics, n = 5 (D) The ratio of CD86/CD163 in the tissue around the OVA scaffold. Data are shown as means ± SD. Statistical analysis: $*p<0.05$, $**p<0.01$, $***p<0.001$, *ns* no significance.

and E2 groups was significantly lower than that of the normal group, but the other groups showed no difference from the normal group. The two-week CD163 fluorescence intensities of the E5/70%, E10/70%, and E4 groups were significantly higher than that of the control group, while the fluorescence intensity of CD163 in 20 kV 20 μL/min, 20 kV 25 μL/min, and E2 groups was slightly higher than that of the normal group, but was not significantly different from the normal group.

These results suggested that M1 macrophages could not be activated rapidly around OVA implants to generate an inflammatory response, but OVA implants favored the recruitment of M2 macrophages. The proportion of M1/M2 macrophages serves as one of the indicators of the inflammation degree in local tissues, and the ratio of M1/M2 macrophages has a greater potential in inflammation and tissue injury repair. In general, the better the biocompatibility, the smaller the M1/M2 macrophage ratio of the biomaterial. As shown in Fig. S10D, the CD86/CD163 ratio in the tissues around the OVA implants was significantly lower than that in the normal group after 1 w of implantation, and the CD86/CD163 ratio was the lowest in the 20 kV 20 μL/min group. In Fig. 5D, the CD86/CD163 ratio in the tissues surrounding the implants in the 20 kV 25 μL/min group was slightly lower than that in the normal group 2 w after implantation, but there was no significant difference, and the other groups displayed significantly lower ratio than that in the normal group, with the lowest CD86/CD163 ratio appeared in the E5/70% group. These results indicated that there was no significant inflammatory response around the OVA implants with the extension of time.

2.5. Immune cell proliferation response

To investigate the implant inflammatory response at 1 w and 2 w, the concentrations of the inflammatory factors IL-10 and TNF-α in the tissues surrounding the implants were determined. As shown in Fig. 6A, the concentrations of IL-10 in the tissues surrounding the OVA implants were significantly higher than normal tissues after 1 w of implantation, and the concentrations of IL-10 in the E5/70% and E2 groups were higher than those of the other implants, with the highest concentration of IL-10 of up to 5575.59 pg/mL in the E2 group. After 2 w of implantation, the concentrations of IL-10 in the tissues surrounding the three forms of OVA implants were still higher than normal tissues. However, the concentrations of IL-10 in the E5/70%, E10/70%, and 20 kV 20 μL/min groups were substantially lower after 2 w of implantation compared with 1 w of implantation. As shown in Fig. 6B, the concentration of TNF-α in the tissues surrounding the E4 group was not significantly different from that of normal tissues after 1 w of implantation, while the other five groups were significantly higher than that of normal tissues, and the highest concentration of TNF-α was found in the E10/70% group, which was up to 2348.79 pg/mL. After 2 w of implantation, the concentration of TNF-α in the E2 group was increased compared with that of implantation for 1 w, and, the TNF-α concentration in the other five groups was slightly lower than that of implantation for 1 w. In addition, the concentration of IL-10 was significantly higher than that of TNF-α at both the 1 w and 2 w. To further investigate the immune cell proliferative response of the OVA implants, CD3 fluorescence staining was performed on the peri-implant tissues (Fig. 6C), the fluorescence intensities of CD3-labeled cells were lower at the 1st week subcutaneous tissues than that at the 2nd week, suggesting that the T-lymphocyte infiltration was increased with the extension of time. As shown in Fig. 6D and E, the results indicated that the CD3 fluorescence intensity at the subcutaneous transplantation site of all OVA implants was not significantly different from that of the surrounding tissues, indicating no immunogenic. The

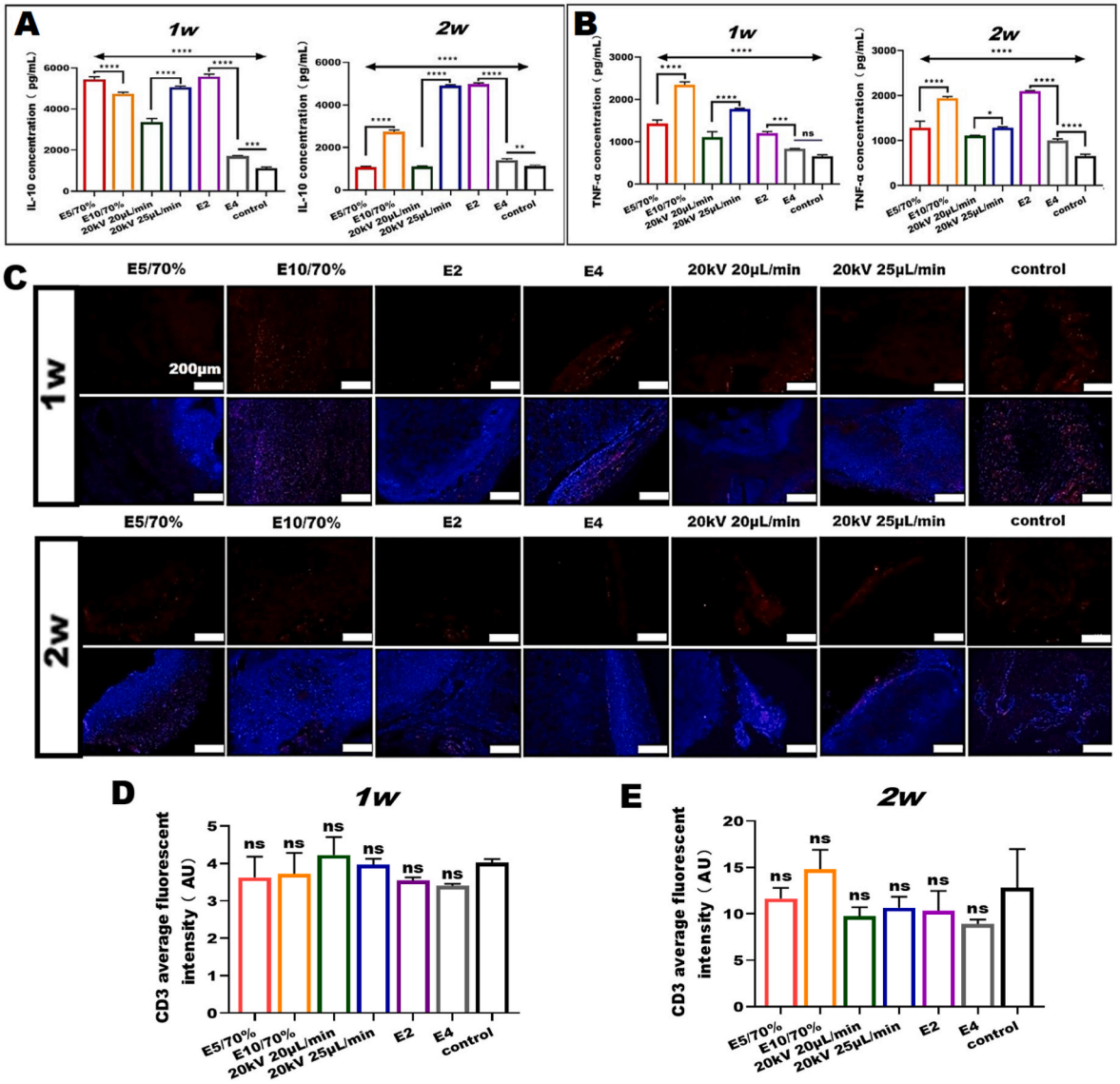

Fig. 6. Inflammatory factors and immune cells of the OVA implants for 1 week and 2 weeks, including E5/70%, E10/70%, 20 kV 20 μL/min, 20 kV 25 μL/min, E2, E4 and normal tissue, respectively. (A) The concentration of IL-10 in the tissue around the implant, n = 3 (B) The concentration of TNF-α, n = 3 (C) Immunofluorescence staining using CD3 antibody and DAPI for analyzing immune cell proliferation response, (D) Quantitative statistics of the average fluorescence intensity of CD3 in one week, n = 5 (E) Quantitative statistics of the average fluorescence intensity of CD3 in two weeks, n = 5. Data are shown as means ± SD. Statistical analysis: ****$p < 0.0001$, *ns* no significance.

immune-fluorescence intensity of OVA sponge scaffolds was slightly lower compared with that of the fiber scaffolds group and OVA membrane group at the two time points. And the immunofluorescence intensity of the fibrous scaffolds was slightly higher than that of the other two forms of implants in the 1st week but slightly higher than that of the other groups at the 2nd week, while there was no significant difference among the groups.

2.6. Growth of the nerve fiber

To investigate the effect of OVA implants on healing after tissue injury, nerve fiber growth at the subcutaneous injury was detected using immunofluorescence staining. As shown in Fig. 7A, NF200-specific labeled nerve fibers were shown in green. Normal nerve fibers were used as the control group. As shown in Fig. 7B and C, the fluorescence intensity of nerve fibers in the E10/70% and 20 kV 25 μL/min groups was lower than that of the control group in the one-week time point, indicating that in a short period of time, the growth of nerve fibers in the E10/70% and 20 kV 25 μL/min groups failed to reach that of the normal group. The fluorescence intensity of nerve fibers in the 20 kV 20 μL/min group was the highest. The fluorescence intensity of nerve fibers in the six OVA implants groups was higher than that in the control group at the two-week time point, indicating that OVA implants could promote nerve fiber regeneration at the injury site. In addition, the E5/70% group showed the highest nerve fiber fluorescence intensity. Taken together, these results indicate that the E5/70% group and the 20 kV 20 μL/min group promoted nerve fiber regeneration best.

2.7. Transcriptome sequencing and reverse transcription-polymerase chain reaction (RT-PCR)

As shown in Fig. 8A, the concentration of NGF released from Schwann cells in the control group was only 39.22 ng/L, but was higher in the OVA implants groups. The highest concentration of NGF was found in the 20 kV 20 μL/min group, which was 55.52 ng/L. Fig. 8B shows that the control group had a total of 96 genes up-regulated and 93

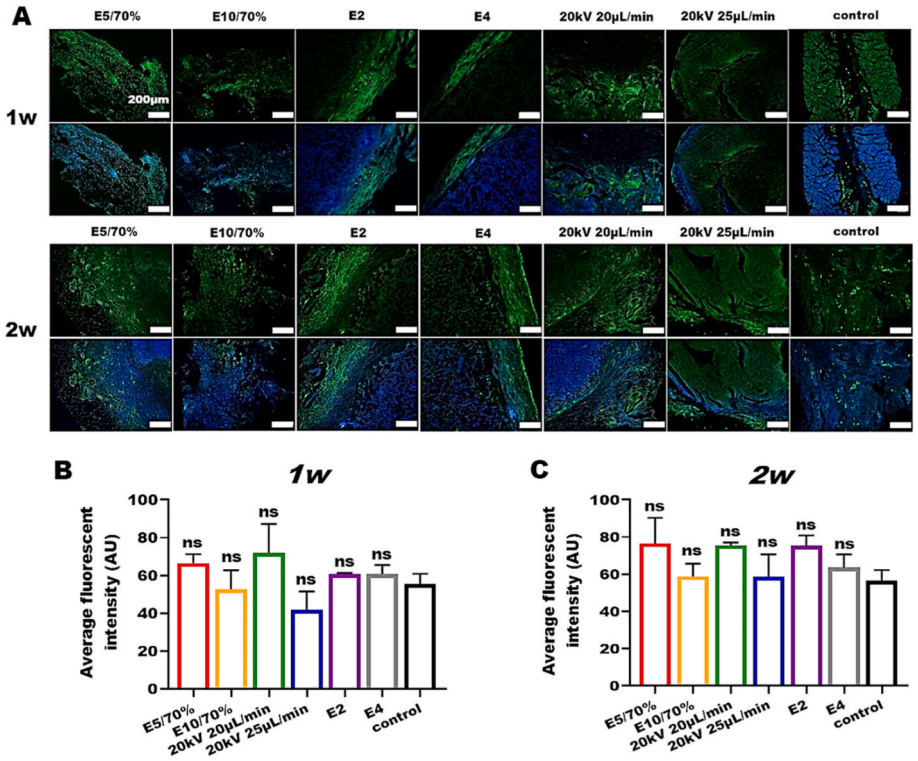

Fig. 7. Nerve fiber of the OVA implants for 1 week and 2 weeks, including E5/70%, E10/70%, 20 kV 20 μL/min, 20 kV 25 μL/min, E2, E4 and normal tissue, respectively. (A) Immunofluorescence staining using NF200 antibody and DAPI for analyzing nerve fiber, (B) Quantitative statistics of the average fluorescence intensity of nerve fiber in one week, n = 3 (C) Quantitative statistics of the average fluorescence intensity of nerve fiber in two weeks, n = 3. Data are shown as means ± SD. Statistical analysis: *ns* no significance.

genes down-regulated compared with the 20 kV 20 μL/min group, 155 genes up-regulated and 101 genes down-regulated compared with the E5/70% group, and 287 genes up-regulated and 356 genes down-regulated compared to the E2 group. The above differential expression analysis (DEG) were plotted into a volcano map and shown in Fig. S11, with red dots indicating up-regulation of differential genes and blue dots indicating down-regulation of differential genes. By analyzing the biological functions involved in all the up-regulated and down-regulated genes, the major biochemical metabolic pathways and signaling pathways involved in the differential genes in the four groups of samples could be identified, as shown in Fig. S12. The degree of kyoto encyclopedia of genes and genomes (KEGG) enrichment was measured by the number of genes enriched to this pathway by multiple factors, and the results indicated that the expressed genes were mainly involved in the TNF signaling pathway, the PI3K-Akt pathway, the ECM receptor interaction pathway, the MAPK signaling pathway, the cytokine and chemokine signaling pathway, the axon guidance, the cellular adhesion junctions, the nerve regeneration. By screening the results of the above DEGs, the heatmap results are shown in Fig. 8C, the genes related to the biological functions of cell adhesion, proliferation, migration, myelin sheath formation, nerve regeneration, and Ca^{2+} transmembrane exchange were selected to re-analyze the differential gene class clustering, the E2 group had more genes positively regulated in cell proliferation, migration, and Ca^{2+} transmembrane exchange, the control group had the least number of genes positively regulated, suggesting that OVA sponge scaffolds were able to modulate differential expression of the relevant genes. RT-PCR was further used to detect the mRNA levels of key genes related to chemotactic response, nerve regeneration and axonal growth. As shown in Fig. 8D, the mRNA levels of EGR2, Met and MPZ were significantly up-regulated in the experimental groups compared with the control group, the mRNA level of ERG2 was higher in the E2 group than other groups, the mRNA level of Met was higher in the 20 kV 20 μL/min group than other groups, and the mRNA level of YAP was significantly higher in the E5/70% group than the control group.

3. Discussion

Numerous biomaterials have been widely used for peripheral nerve regeneration in the last two decades and achieve considerable progress [37]. Artificial nerve implants prepared from natural and synthetic biomaterials have been reported to be effective in promoting regeneration of PNI, but they still do not fully meet the clinical needs currently [10,38]. OVA is the main protein component in egg white, which has good biodegradability and nutritional properties, and can be degraded into active peptide fragments with immunomodulatory functions [14,16]. The extracted OVA was found to promote cell transformation [39], thus, the application of non-toxic OVA has potential application for the treatment of PNI. In this study, OVA membrane, OVA fiber scaffolds and OVA sponge scaffolds were successfully prepared by using casting method, electrospinning and freeze-drying technology. The results showed that the EDC could cross-link the OVA implants well regardless of the spatial structure, and the physicochemical properties and biocompatibility of the cross-linking OVA implants were excellent and there was no obvious cytotoxicity. In vitro experiments showed that OVA implants were able to regulate the proliferation and morphological changes of Schwann cells, and the fiber scaffolds in the 20 kV 20 μL/min group promoted the secretion of more NGF by Schwann cells. In vivo experiments showed that OVA implants could promote vascularization, possessed good histocompatibility without inflammatory reaction and immunogenicity, and the E5/70% and 20 kV 20 μL/min groups were more conducive to the healing of nerve injury. Mechanism study showed that OVA implants promote DEGs related to Schwann cell proliferation, adhesion, migration, myelin formation, nerve regeneration, Ca^{2+} transmembrane exchange. The study provides an important reference for the development of artificial implant materials for the repair of PNI.

The mechanical properties of untreated OVA implants are poor and

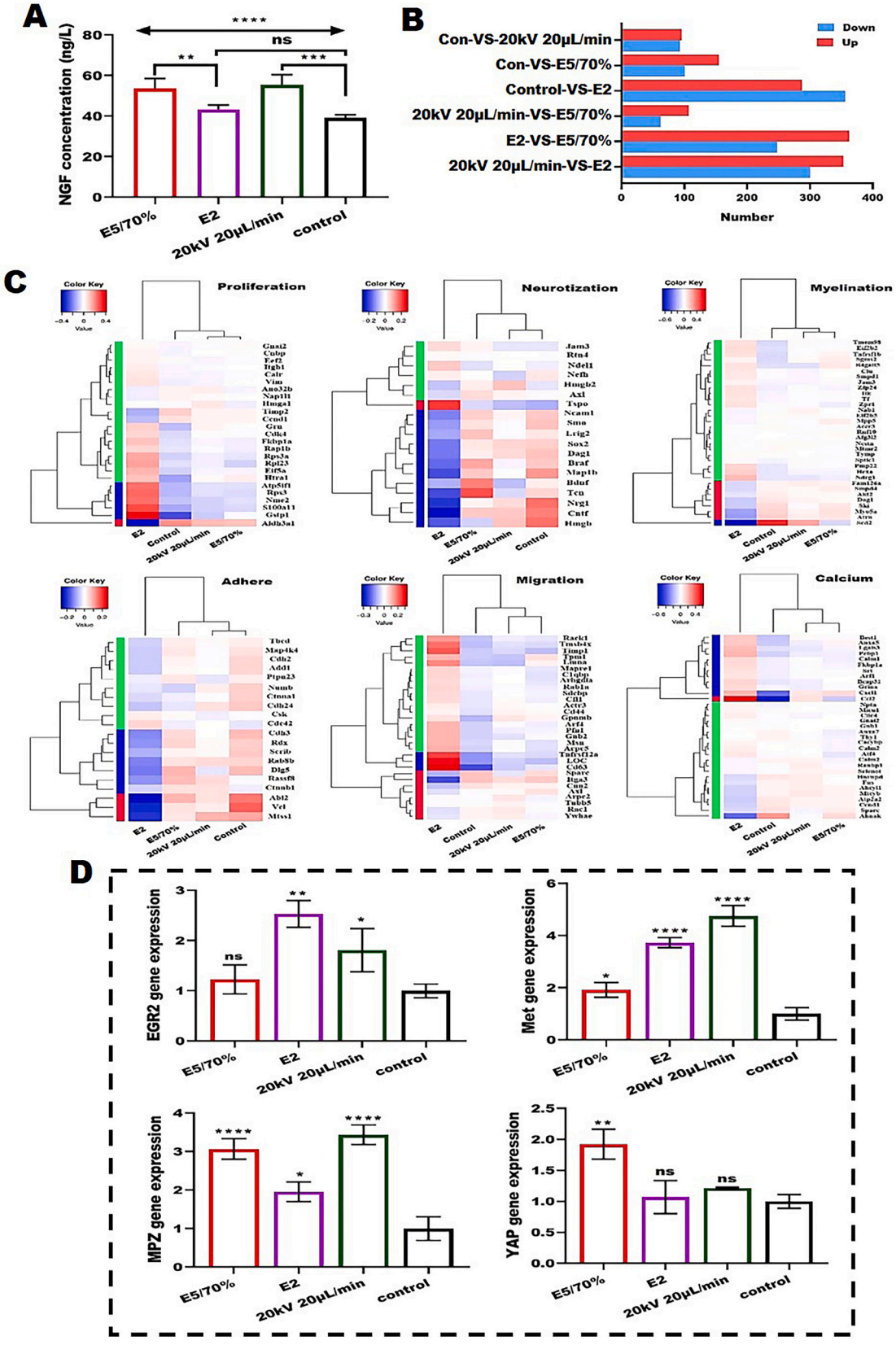

Fig. 8. Transcriptome profiles of Schwann cells on E5/70% (OVA membrane), E2 (OVA lyophilized scaffold), 20 kV 20 μL/min (OVA fiber scaffold), control (the pure slide) groups. (A) The concentration of NGF in cell supernatant, n = 3 (B) Quantitative statistics of up-and down-regulation of differential gene expression in OVA scaffold group samples, (C) Heatmap of DEGs of Schwann cells among different groups, (D) mRNA expressions results of the Schwann cells using RT-PCR analysis, n = 3. Data are shown as means ± SD. Statistical analysis: $^{*}p<0.05$, $^{**}p<0.01$, $^{***}p<0.001$, $^{****}p<0.0001$, *ns* no significance.

could not satisfy the request as tissue engineered scaffolds, therefore the cross-linking of OVA implants is needed to improve their physical and chemical properties [19,21]. Although physical cross-linking ensures the biosafety of the scaffolds, chemical cross-linking was used in this study to improve the performance of OVA implants due to its insufficient cross-linking strength [40,41]. The commonly used chemical cross-linking agents include *N*,*N*′-methylenebisacrylamide, glutaraldehyde, formaldehyde, etc, but most of these chemicals are cytotoxic and not suitable for use in tissue engineering [42], while EDC with excellent biocompatibility and non-toxicity is a zero-degree cross-linking agent commonly used in the field of protein biochemistry, which can be used as an activator to catalyze the formation of amide bonds between carboxyl and amine groups, and is widely used in the biological and chemical fields [43]. FTIR and XPS results demonstrated the cross-linking effect of EDC on OVA implants. EDC cross-linking improved the mechanical properties of OVA implants while maintaining their respective morphological structures and achieving controlled degradation. Typically, protein-based biomaterials are usually brittle and have low structural stability, which is not favorable for biomedical engineering applications [44,45], addition of plasticizers is a method to solve the above problem, glycerol is a non-volatile organic compound which could increase the elongation, processability and toughness of the polymers [46]. Therefore, in this study, glycerol was selected as a plasticizer, and EDC (1 mM, 5 mM, and 10 mM) was used as crosslinker, a novel OVA membrane was prepared in different ethanol concentrations (50%, 70%, and 100%). It was found that as the concentration of the crosslinker increased, the water absorption capacity of the membranes decreased due to the reduction of interchain voids. In addition, the membrane prepared in 100% ethanol underwent rapid degradation in water, which was speculated to be possibly due to excessive cross-linking of the OVA, and the rapid denaturation of the surface OVA proteins by 100% ethanol reduced the ability of the EDC to penetrate into the deeper layers of the OVA membrane [39]. In addition, 50% ethanol cross-linking could not maintain the stable structure of the OVA membrane, thus 70% ethanol was chosen for cross-linking the samples. Morphological observations, tensile tests and UV spectral scans showed that the OVA membrane had good mechanical properties, gas exchange and easy observation for tissue repair. Moreover, the membrane has good biocompatibility and is suitable for subsequent cell culture. Schwann cell culture results showed that the cell growth status of the E5/70% and E10/70% groups was better than the other groups, and the OVA membrane could significantly promote cell growth.

In addition to the material bulk and its chemical composition, the physical and morphological characteristics of the biomaterials surface also play a role in modulating cell behavior in tissue repair and regeneration [23,47]. Protein nanofibers are superior to other polymer fibers because they are biocompatible, tunable biodegradation, good mechanical integrity, and the adjusted size and morphology. Therefore, protein nanofibers are widely used in biomedical applications such as tissue engineering, regenerative medicine, drug delivery, and wound dressings [48]. OVA is a globular protein, and undesirable molecular entanglements caused by the molecular structure reduce their spinnability and hinder fiber development. The process of electrospinning using OVA alone is very unstable or difficult to carry out, resulting in low or no filament production [49]. Several studies loaded OVA onto other electrospun fibers for controlled drug release studies. For example, Yang et al. used electrospinning to prepare the OVA@Eth-HA-GC/SF nanofibrous mats, which significantly inhibited the growth of tumors in the mouse model, and could be used to efficiently stimulate the immune response in the mouse through transdermal delivery [50]. In this study, new OVA fiber scaffolds were prepared by using electrospinning technology, and a variety of spinning solvents were tried for OVA electrospinning, and it was found that the solubility of OVA in HFIP and *N*,*N*-Dimethylformamide was too low, the use of TFA could be used to prepare electrospinning solution, but the viscosity of the solution was too large, which was easy to clog the needles, the use of formic acid could be used to prepare electrospinning solution but it did not form filament, and the viscosity of the electrospinning solution prepared by using dimethyl sulfoxide as the solvent was too low. The low solubility may be due to intermolecular interactions of OVA in organic solvents, which promote electrostatic interactions as well as hydrogen bond formation, leading to protein aggregation [51]. Excessive viscosity may be due to the fact that the solvent used denatures the protein, destroying the spatial structure of the protein, exposing the hydrophobic groups within the molecule, and the aggregation of hydrophobic bonds leading to excessive viscosity [49]. Finally, under the spinning parameter conditions of OVA solution concentration of 10%, electrospinning time of 5 min, receiving distance of 15 cm, needle type of 20, and voltage of more than 20 kV, the randomly aligned OVA fibers were successfully prepared by mixing HFIP and TFA as electrospinning solvents in a ratio of 2:1, which resulted in a high filament output, uniform fibers without droplet appearances, and adjustable fiber diameters. The results showed that both groups of OVA fiber scaffolds, i.e. 20 kV 20 μL/min and 20 kV 25 μL/min, had good hydrophilicity and could better promote the adhesion and proliferation of Schwann cells. In addition, it was found that the orientation of nanofibers plays a crucial role in determining the cell proliferation and adhesion rate, can promote the growth of cells along with the nanofibers direction [34]. Therefore, the OVA fibers can be subsequently subjected to further process improvements.

OVA scaffolds have already been applied for bone or soft tissue repair. Luo et al. prepared porous OVA scaffolds with adjustable properties using different cross-linking agents, and the study demonstrated the feasibility of OVA-based scaffolds as cell carriers for soft tissue engineering applications [17]. In this study, OVA was fabricated into sponge scaffolds with regular porous microstructures and appropriate mechanical properties by freeze-drying, and cross-linked by EDC to further increase the mechanical properties of the scaffolds. The OVA sponge scaffolds were subjected to 50 cycles of compression testing, and the results showed that the scaffolds possessed better shape memory properties, and exhibited suitable structural stability by adjusting the cross-linking strength. Therefore, the scaffolds will be stable for peripheral nerve injury repair. In addition, by increasing the crosslink density, the scaffolds can withstand the hydrodynamic forces of the medium, resulting in a higher swelling ratio. However, increasing the crosslinking concentration to a certain value resulted in a decrease in the number of hydrophilic groups, which led to a decrease in the swelling ratio [52]. MTT and H&E staining results showed that the E2 and E4 groups had good biocompatibility and the porous structure of the sponge scaffolds favored the growth and infiltration of Schwann cells.

To evaluate the safety and biocompatibility of OVA implants (membrane, fiber scaffolds, and sponge scaffolds) in vivo, six groups (E5/70%, E10/70%, E2, E4, 20 kV 20 μL/min, and 20 kV 25 μL/min groups) were optimally selected for subcutaneous implantation in mice. One week and two weeks after subcutaneous implantation in ICR mice, subcutaneous tissues were removed for histological analysis to assess the tissue response to the implants. After OVA implantation, there was no significant formation of a fibrous capsule membrane between the implants and the subcutaneous tissue, indicating that the OVA implants had good histocompatibility. Biomaterials with good biocompatibility can induce macrophage polarization toward M2-type macrophages, which are favorable for tissue repair and regeneration, and the ratio of M1/M2 macrophages serves as one of the indicators of the degree of inflammation in local tissues, the better the biomaterials with good biocompatibility, the smaller the M1/M2 macrophage ratio is [53]. Immunohistochemical analysis of macrophages in this study showed that subcutaneous tissue transplanted with OVA implants had lower inflammatory responses compared with surrounding tissues. M1 macrophages were not rapidly activated and inflammatory responses around OVA implants was not generated. Moreover, the OVA implants favor the accumulation of M2 macrophages. The macrophage ratios of M1/M2 in the E5/70% group and the 20 kV 20 μL/min group were smaller, indicating better biocompatibility. IL-10 is a cytokine with

anti-inflammatory activity, and IL-10 mainly inhibits nuclear factor kappa-B (NF-kB) target genes in macrophages, the MAPK signaling pathway is one of the key pathways regulating IL-10 [54]. TNF-α is an inflammatory factor secreted by immune cells during the onset of acute inflammation, which is responsible for a variety of intracellular signaling and promotes cell necrosis or apoptosis [55]. The concentrations of IL-10 and TNF-α in the tissues around the implant were measured, and IL-10 concentration was significantly higher than TNF-α in both 1 w and 2 w, indicating the OVA implants could promote the subsidence of inflammatory response. The IL-10 concentration of in the OVA sponge scaffolds of E2 group was the highest, which is more conducive to the repair of tissue damage. T-lymphocytes play a role in immunomodulation and influence tissue healing, the decrease or increase in T-lymphocytes suggests a slowing down or worsening of inflammation at the site of injury [56]. CD3 labels almost all T lymphocytes, and the immunohistochemical results of CD3 in this study suggested that OVA implants did not exacerbate the inflammatory response at the implantation site, which had a favorable impact on tissue repair and healing. However, the specific mechanisms regarding the role of T-lymphocytes in peripheral nerve regeneration and repair are currently unknown.

Both tissue regeneration repair and scar healing involve nerve repair, which is a critical stage in the tissue healing process [57]. The growth of neural axons is affected by various regulatory factors and extracellular matrix in scar tissue and granulation tissue. For example, during tissue healing, cell growth factors secreted by the relevant cells, such as vascular endothelial growth factor (VEGF), transforming growth factor-1 (TGF-1), platelet-derived growth factor (PDGF), and fibroblast growth factors (FGFs) can promote cell growth and differentiation, which have a significant role in wound healing [58]. In this study, immunohistochemical analysis was performed on the subcutaneous injury site, and the fluorescence intensity of nerve fibers in the E10/70% and 20 kV 25 μL/min groups was lower than that of normal tissues at the one-week time point, indicating that the amount of nerve fiber growth promoted by the membrane in the E10/70% group and the fiber scaffolds in the 20 kV 25 μL/min group failed to reach the level of normal tissues in a short period of time. The fluorescence intensity of nerve fibers in all OVA implants groups was higher than that in the control group at the two-week time point, indicating that OVA implants could effectively promote the regeneration of nerve fibers at the injury after a period of time. And the E5/70% group membrane and 20 kV 20 μL/min group fiber scaffolds were more conducive to promoting nerve fiber regeneration. NGF is a neurotrophic factor innervated by sensory and sympathetic neuronal projections that stimulates synaptic growth and nerve regeneration after injury [59]. Here, Schwann cells were cultured on the implants of E5/70%, E2 and 20 kV 20 μL/min and cultured for 3 days to investigate the effect on the secretion of NGF involved in the tissue healing process, and the results showed that the fiber scaffolds of the 20 kV 20 μL/min group promoted the Schwann cells to secrete more NGF than other groups.

It has been reported that OVA induced increased levels of NF-kB and IkB-α phosphorylation, expression of NF-kB target genes, and cytokine-associated janus kinase 2 (JAK2)/signal transducer and activator of transcription 3 (STAT3) phosphorylation. In addition, activated JAK2/STAT3 signaling increased the number of Ki67 proliferating cells and the target genes expression of developmental pathway in an inflammatory model, thereby promoting tissue regeneration [51]. In this study, the results of high-throughput sequencing showed that the E2 group sponge scaffolds promoted the DEGs related to functions such as Schwann cell proliferation, migration, and Ca^{2+} transmembrane exchange. The E5/70% membrane promoted the DEGs related to functions such as Schwann cell adhesion and nerve regeneration. These differential genes are involved in a variety of biological processes, including TNF signaling pathway, MAPK signaling pathway, PI3K-Akt pathway, ECM receptor interaction pathway, cytokine and chemokine signaling pathway, cell adhesion and proliferation, nerve regeneration, myelin sheath formation, and Ca^{2+} transmembrane exchange. In addition, RT-PCR results showed that the prepared OVA implants could significantly upregulate the expression of EGR2, Met, MPZ and YAP. Combining the results of mRNA-Sequence and RT-PCR experiments, we proposed a possible mechanism by which different forms of OVA implants regulate peripheral nerve regeneration (Fig. 9). PI3K binding to epidermal growth factor receptor (EGFR) changes the structure of Akt protein to activate Akt protein, and the activated Akt protein can activate or inhibit downstream activities of related proteins, thus regulating the processes of cell proliferation, differentiation and apoptosis. PI3K can activate the transcription factor inhibitor of kappa B kinase (IKK), which can be phosphorylated to IkB-α protein after activation, causing NF-kB detachment, which is then transferred to the nucleus and binds to the DNA, leading to altered cellular functions [60]. When GTP replaces GDP and binds to Ras, it phosphorylates and activates the downstream pathway Raf, which in turn activates the cascade amplification reaction of serothreonine kinase and ultimately activates extracellular regulated protein kinases (Erk)/MAPK, thus regulating cell adhesion and preventing apoptosis. TNF signaling activates the downstream signaling pathway of NF-kB, which is an important nuclear transcription factor in the cell. The MAPK pathway transmits signals to the nucleus to activate a large number of transcription factors, many of which up-regulate myelination-related genes and proteins in Schwann cells, thereby regulating Schwann cell myelination [61]. Interleukin-17 (IL-17), secreted by helper T cells (Th17) and innate immune cells, among others, is an important pro-inflammatory cytokine, which plays a key role in a variety of inflammatory responses and autoimmune disease processes. IL-17 receptor (IL-17 R) activates downstream MAPK and NF-kB signaling pathways through the signaling complex IL-17 R-Act1-TRAF6. In addition, the activated Ras pathway directly interacts with PI3K, and PI3K activates the downstream Erk pathway. These signaling pathways interact with each other to form a complex microenvironment that regulates cell development and promotes nerve regeneration.

4. Conclusion

In summary, we successfully prepared OVA membranes, OVA fiber scaffolds, and OVA porous sponge scaffolds by using casting, electrospinning, and freeze-drying techniques. The three forms of OVA implants were successfully crosslinked with EDC, which improved the stability and mechanical properties, but did not change the morphology and structure of the grafts. The three forms of OVA implants showed excellent physicochemical properties and were biocompatible without significant toxicity. The OVA implants promoted vascularization, displayed good histocompatibility without inflammatory reaction and immunogenicity. The highest concentration of IL-10 was obtained in the tissues around the sponge scaffolds in the E2 group, and the E5/70% and 20 kV 20 μL/min groups were biocompatible and more conducive to promoting tissue healing. In addition, we found that the sponge scaffolds in the E2 group significantly up-regulated the DEGs related to cell proliferation, migration and Ca^{2+} transmembrane exchange, the E5/70% group significantly up-regulated the expression of genes related to cell adhesion and nerve regeneration, which suggested a possible signaling pathway for the regulation of nerve regeneration by OVA implants. Therefore, the OVA implants developed in this study may have a wide range of applications in peripheral nerve regeneration and other tissue engineering. The study is also expected to provide a theoretical basis for the development and design of novel implant materials for nerve regeneration.

Availability of data and materials

All data have been included in the paper. The datasets used in this study are available from the corresponding author on reasonable request.

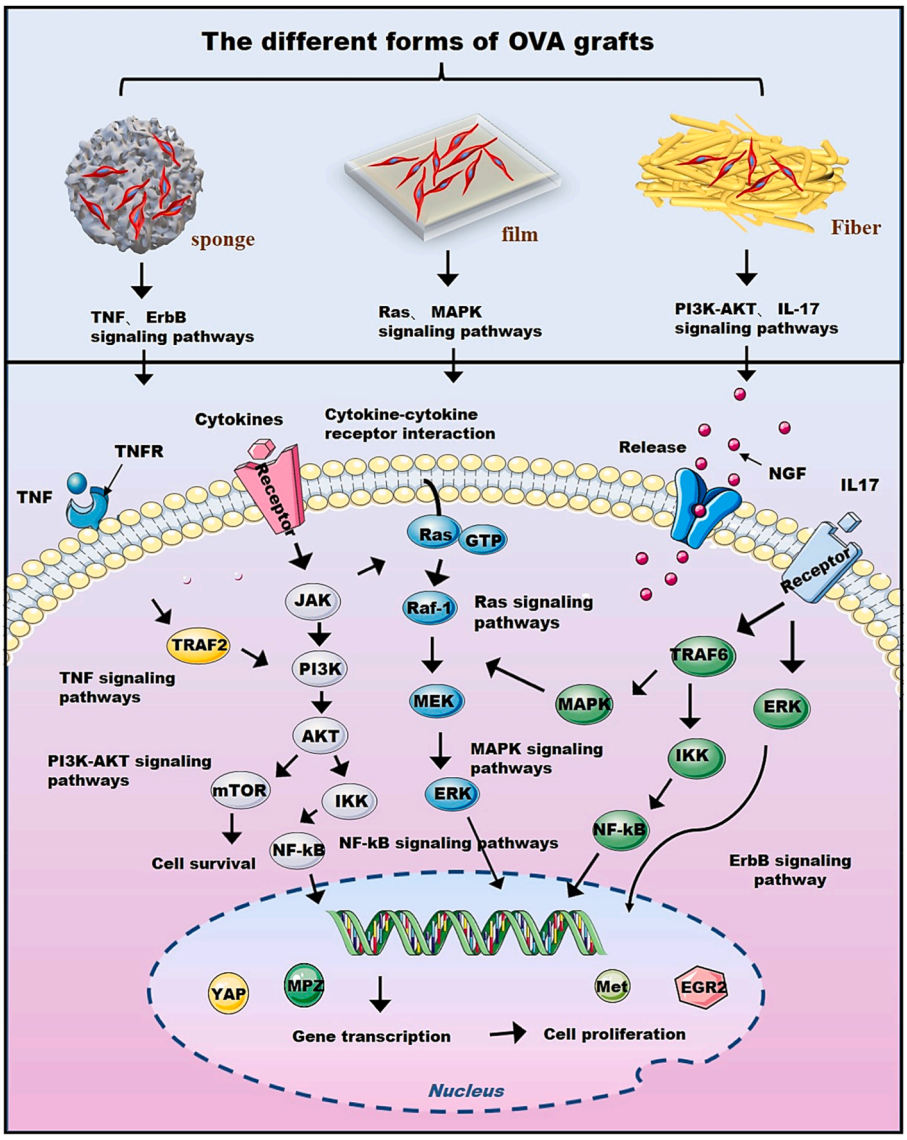

Fig. 9. The possible signal pathways related to cell proliferation, migration, axon growth and myelination of Schwann cells on OVA implants with different spatial structures (membrane, fiber, and lyophilized scaffold).

Ethics approval and consent to participate

All animal experiments were approved by the Ethical Committee of Laboratory Animals of Nantong University (No. S20210302-047). Informed consent was obtained from all subjects involved in the study.

CRediT authorship contribution statement

Tiantian Zheng: Writing – original draft, Methodology, Investigation, Formal analysis, Data curation. **Hongxia Gao:** Visualization, Software, Methodology. **Yaqiong Liu:** Visualization, Software, Formal analysis. **Shaolan Sun:** Formal analysis, Data curation. **Wenchao Guan:** Software, Resources, Project administration. **Linliang Wu:** Software, Investigation, Formal analysis. **Yumin Yang:** Writing – review & editing, Validation, Supervision. **Guicai Li:** Writing – review & editing, Supervision, Resources, Funding acquisition, Conceptualization.

Declaration of competing interest

The authors declare that they have no known competing financial interests or personal relationships that could have appeared to influence the work reported in this paper.

Acknowledgements

The authors gratefully acknowledge the financial support of the National Natural Science Foundation of China (32171352), Special Funds for Provincial Science and Technology Programs (Key R&D Program for Social Development) of Jiangsu Province (BE2023743), Open Research Fund of State Key Laboratory of Advance Technology for Materials Synthesis and Processing (Wuhan University of Technology, 2023-KF-18), Open Research Fund of State Key Laboratory of Bioelectronics, Southeast University (2023-K05), Opening Project of State Key Laboratory of Polymer Materials Engineering (Sichuan University, Sklpme2022-4-01) and 226 High-level Talent Training Project (2nd level, 2022 II-276).

Appendix A. Supplementary data

Supplementary data to this article can be found online at https://doi.org/10.1016/j.bioactmat.2024.01.025.

References

[1] J. Moskow, B. Ferrigno, N. Mistry, D. Jaiswal, K. Bulsara, S. Rudraiah, S. G. Kumbar, Review: bioengineering approach for the repair and regeneration of peripheral nerve, Bioact. Mater. 4 (2019) 107–113, https://doi.org/10.1016/j.bioactmat.2018.09.001.

[2] Y. Qian, H. Lin, Z. Yan, J. Shi, C. Fan, Functional nanomaterials in peripheral nerve regeneration: scaffold design, chemical principles and microenvironmental remodeling, Mater. Today 51 (2021) 165–187, https://doi.org/10.1016/j.mattod.2021.09.014.

[3] B. Gong, X. Zhang, A. Al Zahrani, W. Gao, G. Ma, L. Zhang, J. Xue, Neural tissue engineering: from bioactive scaffolds and in situ monitoring to regeneration, Explorations 2 (2022) 20210035, https://doi.org/10.1002/EXP.20210035.

[4] T. Zheng, L. Wu, S. Sun, J. Xu, Q. Han, Y. Liu, R. Wu, G. Li, Co-culture of Schwann cells and endothelial cells for synergistically regulating dorsal root ganglion behavior on chitosan-based anisotropic topology for peripheral nerve regeneration, Burns Trauma 10 (2022), https://doi.org/10.1093/burnst/tkac030 tkac030.

[5] S. Gao, X. Chen, B. Lu, K. Meng, K.Q. Zhang, H. Zhao, Recent advances on nerve guide conduits based on textile methods, Smart Mater Med 4 (2023) 368–383, https://doi.org/10.1016/j.smaim.2022.12.001.

[6] Y. Zhang, Y. Xu, H. Kong, J. Zhang, H.F. Chan, J. Wang, D. Shao, Y. Tao, M. Li, Microneedle system for tissue engineering and regenerative medicine, Explorations 3 (2023) 20210170, https://doi.org/10.1002/EXP.20210170.

[7] J. Zhang, X. Zhang, C. Wang, F. Li, Z. Qiao, L. Zeng, Z. Wang, H. Liu, J. Ding, H. Yang, Conductive composite fiber with optimized alignment guides neural regeneration under electrical stimulation, Adv. Healthcare Mater. 10 (2021) 2000604, https://doi.org/10.1002/adhm.202000604.

[8] R. Deng, Z. Luo, Z. Rao, Z. Lin, S. Chen, J. Zhou, Q. Zhu, X. Liu, Y. Bai, D. Quan, Decellularized extracellular matrix containing electrospun fibers for nerve regeneration: a comparison between core–shell structured and preblended composites, Advanced Fiber Materials 4 (2022) 503–519, https://doi.org/10.1007/s42765-021-00124-5.

[9] S. Vijayavenkataraman, Nerve guide conduits for peripheral nerve injury repair: a review on design, materials and fabrication methods, Acta Biomater. 106 (2020) 54–69, https://doi.org/10.1016/j.actbio.2020.02.003.

[10] K. Liu, L. Yan, R. Li, Z. Song, J. Ding, B. Liu, X. Chen, 3D printed personalized nerve guide conduits for precision repair of peripheral nerve defects, Adv. Sci. 9 (2022) 2103875, https://doi.org/10.1002/advs.202103875.

[11] H. Wang, H. Wan, Q. Wang, Y. Ma, G. Su, X. Cao, H. Gao, Engineered multifunctional silk fibroin/gelatin hydrogel conduit loaded with miR-29a@ZIF-8 nanoparticles for peripheral nerve regeneration, Smart Mater Med 4 (2023) 480–492, https://doi.org/10.1016/j.smaim.2023.02.002.

[12] Z. Wang, H. Wei, Y. Huang, Y. Wei, J. Chen, Naturally sourced hydrogels: emerging fundamental materials for next-generation healthcare sensing, Chem. Soc. Rev. 52 (2023) 2992–3034, https://doi.org/10.1039/d2cs00813k.

[13] H. Zhang, J. Guo, Y. Wang, L. Shang, R. Chai, Y. Zhao, Natural polymer-derived bioscaffolds for peripheral nerve regeneration, Adv. Funct. Mater. 32 (2022) 2203829, https://doi.org/10.1002/adfm.202203829.

[14] B. Luo, Q.L. Loh, M.T. Chong Wong, N.S. Tan, C. Choong, Bioactivated protein-based porous microcarriers for tissue engineering applications, J. Mater. Chem. B 2 (2014) 7795–7803, https://doi.org/10.1039/c4tb00846d.

[15] Z. Guo, T. Zhang, K. Fang, P. Liu, M. Li, N. Gu, The effect of porosity and stiffness of glutaraldehyde cross-linked egg white scaffold simulating aged extracellular matrix on distribution and aggregation of ovarian cancer cells, Colloids Surf. A Physicochem. Eng. Asp. 504 (2016) 43–52, https://doi.org/10.1016/j.colsurfa.2016.05.050.

[16] S. Jalili-Firoozinezhad, M. Filippi, F. Mohabatpour, D. Letourneur, A. Scherberich, Chicken egg white: hatching of a new old biomaterial, Mater. Today 40 (2020) 193–214, https://doi.org/10.1016/j.mattod.2020.05.022.

[17] B. Luo, C. Choong, Porous ovalbumin scaffolds with tunable properties: a resource-efficient biodegradable material for tissue engineering applications, J. Biomater. Appl. 29 (2015) 903–911, https://doi.org/10.1177/0885328214548881.

[18] N.T. Carpena, C.D.G. Abueva, A.R. Padalhin, B.T. Lee, Evaluation of egg white ovomucin-based porous scaffold as an implantable biomaterial for tissue engineering, J. Biomed. Mater. Res. B Appl. Biomater. 105 (2017) 2107–2117, https://doi.org/10.1002/jbm.b.33750.

[19] H. Gao, Y. Liu, W. Guan, S. Sun, T. Zheng, L. Wu, G. Li, Surface topologized ovalbumin scaffolds containing YIGSR peptides for modulating Schwann cell behavior, Int. J. Biol. Macromol. 253 (2023) 127015, https://doi.org/10.1016/j.ijbiomac.2023.127015.

[20] C. Kojima, Y. Narita, Y. Nakajima, N. Morimoto, T. Yoshikawa, N. Takahashi, A. Handa, T. Waku, N. Tanaka, Modulation of cell adhesion and differentiation on collagen gels by the addition of the ovalbumin secretory signal peptide, ACS Biomater. Sci. Eng. 5 (2019) 5698–5704, https://doi.org/10.1021/acsbiomaterials.8b01505.

[21] S. Jalili-Firoozinezhad, S. Rajabi-Zeleti, P. Mohammadi, E. Gaudiello, S. Bonakdar, M. Solati-Hashjin, A. Marsano, N. Aghdami, A. Scherberich, H. Baharvand, I. Martin, Facile fabrication of egg white macroporous sponges for tissue regeneration, Adv. Healthcare Mater. 4 (2015) 2281–2290, https://doi.org/10.1002/adhm.201500482.

[22] C. Kalirajan, A. Dukle, A.J. Nathanael, T.H. Oh, G. Manivasagam, A critical review on polymeric biomaterials for biomedical applications, Polymers 13 (2021) 3015, https://doi.org/10.3390/polym13173015.

[23] Y. Qian, X. Zhao, Q. Han, W. Chen, H. Li, W. Yuan, An integrated multi-layer 3D-fabrication of PDA/RGD coated graphene loaded PCL nanoscaffold for peripheral nerve restoration, Nat. Commun. 9 (2018) 323, https://doi.org/10.1038/s41467-017-02598-7.

[24] Y. Chen, X. Dong, M. Shafiq, G. Myles, N. Radacsi, X. Mo, Recent advancements on three-dimensional electrospun nanofiber scaffolds for tissue engineering, Advanced Fiber Materials 4 (2022) 959–986, https://doi.org/10.1007/s42765-022-00170-7.

[25] K. Klimek, M. Tarczynska, W. Truszkiewicz, K. Gaweda, T.E.L. Douglas, G. Ginalska, Freeze-dried curdlan/whey protein isolate-based biomaterial as promising scaffold for matrix-associated autologous chondrocyte transplantation—a pilot in-vitro study, Cells 11 (2022) 282, https://doi.org/10.3390/cells11020282.

[26] C.M. Brougham, T.J. Levingstone, N. Shen, G.M. Cooney, S. Jockenhoevel, T. C. Flanagan, F.J. O'Brien, Freeze-drying as a novel biofabrication method for achieving a controlled microarchitecture within large, complex natural biomaterial scaffolds, Adv. Healthcare Mater. 6 (2017) 1700598, https://doi.org/10.1002/adhm.201700598.

[27] G. Li, C. Xue, H. Wang, X. Yang, Y. Zhao, L. Zhang, Y. Yang, Spatially featured porous chitosan conduits with micropatterned inner wall and seamless sidewall for bridging peripheral nerve regeneration, Carbohydr. Polym. 194 (2018) 225–235, https://doi.org/10.1016/j.carbpol.2018.04.049.

[28] T. Zheng, L. Wu, J. Xu, S. Sun, W. Guan, Q. Han, L. Zhang, X. Gu, Y. Yang, G. Li, YR/DFO@DCNT functionalized anisotropic micro/nano composite topography scaffolds for accelerating long-distance peripheral nerve regeneration, Compos. B Eng. 246 (2022) 110242, https://doi.org/10.1016/j.compositesb.2022.110242.

[29] Y. Mu, F. Wu, Y. Lu, L. Wei, W. Yuan, Progress of electrospun fibers as nerve conduits for neural tissue repair, Nanomedicine 9 (2014) 1869–1883, https://doi.org/10.2217/NNM.14.70.

[30] G. Zhou, Y. Chen, F. Dai, X. Yu, Chitosan-based nerve guidance conduit with microchannels and nanofibers promotes schwann cells migration and neurite growth, Colloids Surf. B Biointerfaces 221 (2023) 112929, https://doi.org/10.1016/j.colsurfb.2022.112929.

[31] L. Cheng, Y. Wang, G. Sun, S. Wen, L. Deng, H. Zhang, W. Cui, Hydration-enhanced lubricating electrospun nanofibrous membranes prevent tissue adhesion, Research 2020 (2020), https://doi.org/10.34133/2020/4907185. UNSP 4907185.

[32] W. Xue, W. Shi, Y. Kong, M. Kuss, B. Duan, Anisotropic scaffolds for peripheral nerve and spinal cord regeneration, Bioact. Mater. 6 (2021) 4141–4160, https://doi.org/10.1016/j.bioactmat.2021.04.019.

[33] Y. Chen, X. Dong, M. Shafiq, G. Myles, N. Radacsi, X. Mo, Recent advancements on three-dimensional electrospun nanofiber scaffolds for tissue engineering, Advanced Fiber Materials 4 (2022) 959–986, https://doi.org/10.1007/s42765-022-00170-7.

[34] G. Li, T. Zheng, L. Wu, Q. Han, Y. Lei, L. Xue, L. Zhang, X. Gu, Y. Yang, Bionic microenvironment-inspired synergistic effect of anisotropic micro-nanocomposite topology and biology cues on peripheral nerve regeneration, Sci. Adv. 7 (2021) eabi5812, https://www.science.org.

[35] Q. Ao, A. Wang, W. Cao, L. Zhang, L. Kong, Q. He, Y. Gong, X. Zhang, Manufacture of multimicrotubule chitosan nerve conduits with novel molds and characterization in vitro, J. Biomed. Mater. Res. 77 (2006) 11–18, https://doi.org/10.1002/jbm.a.30593.

[36] A. Wang, Q. Ao, Y. Wei, K. Gong, X. Liu, N. Zhao, Y. Gong, X. Zhang, Physical properties and biocompatibility of a porous chitosan-based fiber-reinforced conduit for nerve regeneration, Biotechnol. Lett. 29 (2007) 1697–1702, https://doi.org/10.1007/s10529-007-9460-0.

[37] Y. Kong, J. Xu, W. Guan, S. Sun, Y. Yang, G. Li, Tailoring the elasticity of nerve implants for regulating peripheral nerve regeneration, Smart Mater Med 4 (2023) 266–285, https://doi.org/10.1016/j.smaim.2022.11.004.

[38] A. Escobar, A. Serafin, M.R. Carvalho, M. Culebras, A. Cantarero, A. Beaucamp, R. L. Reis, J.M. Oliveira, M.N. Collins, Electroconductive poly(3,4-ethylenedioxythiophene) (PEDOT) nanoparticle-loaded silk fibroin biocomposite conduits for peripheral nerve regeneration, Adv. Compos. Hybrid Mater. 6 (2023) 118, https://doi.org/10.1007/s42114-023-00689-2.

[39] M. Shojaee, F. Navaee, S. Jalili-Firoozinezhad, R. Faturechi, M. Majidi, S. Bonakdar, Fabrication and characterization of ovalbumin films for wound dressing applications, Mater. Sci. Eng. C 48 (2015) 158–164, https://doi.org/10.1016/j.msec.2014.11.063.

[40] D. Rozbeský, M. Rosůlek, Z. Kukačka, J. Chmelík, P. Man, P. Novák, Impact of chemical cross-linking on protein structure and function, Anal. Chem. 90 (2018) 1104–1113, https://doi.org/10.1021/acs.analchem.7b02863.

[41] L. Rebers, R. Reichsöllner, S. Regett, G.E.M. Tovar, K. Borchers, S. Baudis, A. Southan, Differentiation of physical and chemical cross-linking in gelatin methacryloyl hydrogels, Sci. Rep. 11 (2021) 3256, https://doi.org/10.1038/s41598-021-82393-z.

[42] J. Skopinska-Wisniewska, M. Tuszynska, E. Olewnik-Kruszkowska, Comparative study of gelatin hydrogels modified by various cross-linking agents, Materials 14 (2021) 1–17, https://doi.org/10.3390/ma14020396.

[43] N. Lehmann, T. Christ, A. Daugs, O. Bloch, S. Holinski, EDC cross-linking of decellularized tissue: a promising approach? Tissue Eng. 23 (2017) 675–682, https://doi.org/10.1089/ten.tea.2016.0416.

[44] L. Nie, R. Hou, A. Shavandi, Editorial: advances in protein-based biomaterials for tissue engineering, Front. Bioeng. Biotechnol. 10 (2022) 1022733, https://doi.org/10.3389/fbioe.2022.1022733.

[45] C. Romo-valera, P. Guerrero, J. Arluzea, J. Etxebarria, K. de la Caba, N. Andollo, Cytocompatibility and suitability of protein-based biomaterials as potential candidates for corneal tissue engineering, Int. J. Mol. Sci. 22 (2021) 3648, https://doi.org/10.3390/ijms22073648.

[46] Z.Y. Ben, H. Samsudin, M.F. Yhaya, Glycerol: its properties, polymer synthesis, and applications in starch based films, Eur. Polym. J. 175 (2022) 111377, https://doi.org/10.1016/j.eurpolymj.2022.111377.

[47] L. Zhan, J. Deng, Q. Ke, X. Li, Y. Ouyang, C. Huang, X. Liu, Y. Qian, Grooved fibers: preparation principles through electrospinning and potential applications, Advanced Fiber Materials 4 (2022) 203–213, https://doi.org/10.1007/s42765-021-00116-5.

[48] M. Ansari, K.P. Prajapati, B.G. Anand, P. Chaudhuri, S. Mittal, K. Kar, Construction of chemoreactive heterogeneous nanofibers through strategic coassembly of different proteins, Mater Today Nano 22 (2023) 100317, https://doi.org/10.1016/j.mtnano.2023.100317.

[49] W. Nuansing, D. Frauchiger, F. Huth, A. Rebollo, R. Hillenbrand, A.M. Bittner, Electrospinning of peptide and protein fibres: approaching the molecular scale, Faraday Discuss 166 (2013) 209–221, https://doi.org/10.1039/c3fd00069a.

[50] X. Yang, X. Wang, H. Hong, G. Elfawal, S. Lin, J. Wu, Y. Jiang, C. He, X. Mo, G. Kai, H. Wang, Galactosylated chitosan-modified ethosomes combined with silk fibroin nanofibers is useful in transcutaneous immunization, J. Contr. Release 327 (2020) 88–99, https://doi.org/10.1016/j.jconrel.2020.07.047.

[51] C. Kojima, Y. Narita, Y. Nakajima, N. Morimoto, T. Yoshikawa, N. Takahashi, A. Handa, T. Waku, N. Tanaka, Modulation of cell adhesion and differentiation on collagen gels by the addition of the ovalbumin secretory signal peptide, ACS Biomater. Sci. Eng. 5 (2019) 5698–5704, https://doi.org/10.1021/acsbiomaterials.8b01505.

[52] G. Francius, J. Hemmerlé, J. Ohayon, P. Schaaf, J.C. Voegel, C. Picart, B. Senger, Effect of crosslinking on the elasticity of polyelectrolyte multilayer films measured by colloidal probe AFM, Microsc. Res. Tech. 69 (2006) 84–92, https://doi.org/10.1002/jemt.20275.

[53] K.E. Martin, A.J. García, Macrophage phenotypes in tissue repair and the foreign body response: implications for biomaterial-based regenerative medicine strategies, Acta Biomater. 133 (2021) 4–16, https://doi.org/10.1016/j.actbio.2021.03.038.

[54] J.R. Nakkala, Y. Duan, J. Ding, W. Muhammad, D. Zhang, Z. Mao, H. Ouyang, C. Gao, Macrophage membrane-functionalized nanofibrous mats and their immunomodulatory effects on macrophage polarization, Acta Biomater. 141 (2022) 24–38, https://doi.org/10.1016/j.actbio.2021.12.026.

[55] A. Kusnadi, S.H. Park, R. Yuan, T. Pannellini, E. Giannopoulou, D. Oliver, T. Lu, K. H. Park-Min, L.B. Ivashkiv, The cytokine TNF promotes transcription factor SREBP activity and binding to inflammatory genes to activate macrophages and limit tissue repair, Immunity 51 (2019) 241–257.e9, https://doi.org/10.1016/j.immuni.2019.06.005.

[56] K.M. Adusei, T.B. Ngo, K. Sadtler, T lymphocytes as critical mediators in tissue regeneration, fibrosis, and the foreign body response, Acta Biomater. 133 (2021) 17–33, https://doi.org/10.1016/j.actbio.2021.04.023.

[57] Z. Zhu, X. Zhang, H. Hao, H. Xu, J. Shu, Q. Hou, M. Wang, Exosomes derived from umbilical cord mesenchymal stem cells treat cutaneous nerve damage and promote wound healing, Front. Cell. Neurosci. 16 (2022) 913009, https://doi.org/10.3389/fncel.2022.913009.

[58] J. Zhu, Z. Hu, Y. Luo, Y. Liu, W. Luo, X. Du, P. ShengLiang, Z. Luo, J. Hu, Diabetic peripheral neuropathy: pathogenetic mechanisms and treatment, Front. Endocrinol. 14 (2023) 1265372, https://doi.org/10.3389/fendo.2023.1265372.

[59] Q. Min, D.B. Parkinson, X.P. Dun, Migrating Schwann cells direct axon regeneration within the peripheral nerve bridge, Glia 69 (2021) 235–254, https://doi.org/10.1002/glia.23892.

[60] J. Wei, W. Su, Y. Zhao, Z. Wei, Y. Hua, P. Xue, X. Zhu, Y. Chen, G. Chen, Maresin 1 promotes nerve regeneration and alleviates neuropathic pain after nerve injury, J. Neuroinflammation 19 (2022) 32, https://doi.org/10.1186/s12974-022-02405-1.

[61] L.X. Li, J.H. Chu, X.W. Chen, P.C. Gao, Z.Y. Wang, C. Liu, R.F. Fan, Selenium ameliorates mercuric chloride-induced brain damage through activating BDNF/TrKB/PI3K/AKT and inhibiting NF-κB signaling pathways, J. Inorg. Biochem. 229 (2022) 111716, https://doi.org/10.1016/j.jinorgbio.2022.111716.